scientific reports

Check for updates

OPEN

Sodium Tanshinone IIA Sulfonate alleviates vascular senescence in diabetic mice by modulating the A20-NFκB-NLRP3 inflammasome-catalase pathway

Wei Wei[1,2,3]✉, Yan-Yan Heng[4], Fei-Fei Wu[2], Hao-Yu Dong[2], Peng-Fei Zhang[4], Jing-Xia Li[5], Chun-Yan Liu[5], Bing-Jie Yang[6], Jia-Ning Fu[6] & Xin-Yue Liang[7]

Diabetes accelerates vascular senescence, which is the basis for atherosclerosis and stiffness. The activation of NOD-like receptor family pyrin domain containing 3 (NLRP3) inflammasome and oxidative stress are closely associated with the deteriorative senescence in endothelial cells (ECs) and vascular smooth muscle cells (VSMCs). For decades, Sodium Tanshinone IIA Sulfonate (STS) has been utilized as a cardiovascular medicine with acknowledged anti-inflammatory and anti-oxidative properties. Nevertheless, the impact of STS on vascular senescence remains unexplored in diabetes. Diabetic mice, primary ECs and VSMCs were transfected with the NLRP3 overexpression/knockout plasmid, the tumor necrosis factor alpha-induced protein 3 (TNFAIP3/A20) overexpression/knockout plasmid, and treated with STS to detect senescence-associated markers. In diabetic mice, STS treatment maintained catalase (CAT) level and vascular relaxation, reduced hydrogen peroxide probe (ROSgreen) fluorescence, p21 immunofluorescence, Senescence β-Galactosidase Staining (SA-β-gal) staining area, and collagen deposition in aortas. Mechanistically, STS inhibited NLRP3 phosphorylation (serine 194), NLRP3 dimer formation, NLRP3 expression, and NLRP3-PYCARD (ASC) colocalization. It also suppressed the phosphorylation of IkappaB alpha (IκBα) and NFκB, preserved A20 and CAT levels, reduced ROSgreen density, and decreased the expression of p21 and SA-β-gal staining in ECs and VSMCs under HG culture. Our findings indicate that STS mitigates vascular senescence by modulating the A20-NFκB-NLRP3 inflammasome-CAT pathway in hyperglycemia conditions, offering novel insights into NLRP3 inflammasome activation and ECs and VSMCs senescence under HG culture. This study highlights the potential mechanism of STS in alleviating senescence in diabetic blood vessels, and provides essential evidence for its future clinical application.

Keywords Diabetic vascular disease, Endothelial cells, Vascular smooth muscle cells, Senescence, NLRP3 inflammasome, Catalase

Diabetic pathological environment accelerates vascular senescence, which is an early manifestation of hypertension, atherosclerosis, and vascular wall stiffness[1–3]. Senescence of endothelial cells (ECs) and vascular smooth muscle cells (VSMCs) plays a crucial role in diabetic vascular disease[4]. High glucose (HG)-induced reactive oxygen species (ROS)-dependent senescence injures endothelial permeability barrier and the ability to synthesize

[1]Department of Pharmacology, Changzhi Medical College, No.161, Jiefang East Street, Changzhi 046000, Shanxi, China. [2]Department of Endocrinology and Institute of Endocrinology and Metabolic Disease, Heping Hospital Affiliated to Changzhi Medical College, No.110, Yanan Road South, Changzhi 046000, Shanxi, China. [3]Department of Clinical Central Laboratory, Heping Hospital Affiliated to Changzhi Medical College, No.110, Yan'an South Road, Changzhi, Shanxi, China. [4]Department of Nephrology Heping Hospital, Affiliated to Changzhi Medical College, No.110, Yanan Road South, Changzhi, Shanxi, China. [5]Department of Anesthesia, Changzhi Medical College, No.161, Jiefang East Street, Changzhi, Shanxi, China. [6]Department of Stomatology, Changzhi Medical College, No.161, Jiefang East Street, Changzhi, Shanxi, China. [7]Department of Medical Imageology, Changzhi Medical College, No.161, Jiefang East Street, Changzhi, Shanxi, China. ✉email: jaywei@czmc.edu.cn

nitric oxide, a signal molecule of vascular relaxation, resulting in aggravation of inflammatory cell infiltration and tension in vascular wall[5–7]. Similarly, HG-induced ROS-dependent senescence leads to the VSMCs phenotypic switch, from contractile phenotype to secretory phenotype, resulting in collagen accumulation, vascular wall remodeling, and stiffness, ultimately leading to loss of vascular elasticity[8–10]. Therefore, oxidative stress is one of the primary causes of inducing senescence and dysfunction in vascular endothelium and media. The mechanism of HG-induced ROS generation is diverse and often associated with inflammation[11].

Recent studies have demonstrated that the activation of the NOD-like receptor family pyrin domain-containing 3 (NLRP3) inflammasome is crucially involved in the process of ECs and VSMCs senescence, as well as in dysfunctional injury induced by the generation of ROS[12–14]. NLRP3 inflammasome is one of the vital components of innate immunity, and has been linked to a number of major human disease[15]. Studies have proven that the activation of NLRP3 inflammasome damages the biological functions of ECs and VSMCs, inducing DNA damage-dependent cell senescence[16–18]. As an important damage-associated molecular pattern, hyperglycemia condition leads to NLRP3 inflammasome activation-related ECs and VSMCs senescence[19–21]. The activation of NLRP3 inflammasome is very likely the key mechanism of premature vascular senescence. However, the mechanism of the NLRP3 inflammasome activation by HG is still unclear, and the relationship between ROS generation and NLRP3 inflammasome still needs further study.

Sodium Tanshinone IIA Sulfonate (STS) is a small molecule drug that is a sulfonic acid product of Tanshinone IIA, extracted from *salvia miltiorrhza* herb[22,23]. STS has been an effective cardiovascular medicine in clinical treatment for years. STS protects endothelial function through anti-oxidative stress and anti-inflammation[24,25]. STS also has an effect on alleviating ECs senescence induced by hydrogen peroxide[26]. STS inhibits HG-induced proliferation and migration of VSMCs, the mechanisms are related to anti-inflammation[27,28]. However, the effect of STS on alleviating VSMCs senescence had not been confirmed yet.

The present study describes how STS reduces vascular senescence by inhibiting NLRP3 inflammasome-dependent oxidative stress in diabetic mice. Additionally, it provides insights into a novel mechanism for activating the NLRP3 inflammasome in ECs and VSMCs under HG culture.

Materials and methods

Animals

The handling of mice complied with the requirements of the Ethics Committee of Changzhi Medical College (DW2022053). Spontaneously diabetic mice (db/db) and their littermate (wild type, WT), male (more pronounced and stable hyperglycemic state), 8 weeks old, were purchased from a standardized laboratory animal supplier (GEMPHARMATECH, Nanjing, China). Random blood glucose (RBG) was detected by commercial kits, blood glucose meter (GM501 Sinocare, Changsha, China). The oral glucose tolerance test (OGTT) was performed by orally administering 2.0 g/kg D-glucose to overnight-fasted mice, blood glucose levels were then determined at 0, 30, 60, 90 and 120 min, as previously described[29]. The plasma glucose concentration in the OGTT tests was detected using a glucose assay kit (S0201S, Beyotime, Shanghai, China).

Primary ECs and VSMCs isolation and culture

According to our previous studies[21,29], primary ECs and VSMCs were isolated from mouse aortas using tissue block adhesion method. Briefly, the mouse was sacrificed (Carbon dioxide asphyxiation), and the aorta was quickly removed without tearing, the adventitia was gently peeled off under an operating microscope (MSD540T, Murzider, Dongguan, China), and the remaining vessel was opened longitudinally and cut into tissue blocks approximately 3 mm square, the tissue blocks were seeded with endothelium and media respectively, and then cultured in Dulbecco's modified Eagle's medium (DMEM, C11885500BT, Giabco, Shanghai, China) containing 15% fetal bovine serum (FBS, BL201A, Biosharp, Hefei, China), penicillin (100 IU/ml) and streptomycin (100 mg/ml) (C0222, Beyotime, Shanghai, China) at 37 °C in a 5% CO_2 humidified incubator. After reaching confluence, ECs and VSMCs were passaged and cultured in low glucose DMEM (5 mM, LG) or high glucose DMEM (30 mM, HG) containing 10% FBS and 100 IU/ml penicillin and 100 mg/ml streptomycin at 37 °C in a humidified incubator with 5% CO_2 for 72 h prior to detecting the senescence-associated markers. The primary ECs and VSMCs in the third to eighth passage were used.

Transfection

Diabetic mice (db/db), primary ECs and VSMCs were transfected by knockout control plasmid (null-KO, sc-418922, Santa Cruz, Shanghai, China), activation control plasmid (null-ACT, sc-437275, Santa Cruz, Shanghai, China), NLRP3-activated plasmid (NLRP3 over-expression, NOE, sc-432122-ACT, Santa Cruz, Shanghai, China), NLRP3-knockout plasmid (NKO, sc-432122, Santa Cruz, Shanghai, China), A20-activated plasmid (A20 over-expression, AOE, sc-423436-ACT, Santa Cruz, Shanghai, China), A20-knockout plasmid (AKO, sc-423436, Santa Cruz, Shanghai, China), to activate/inhibit the expression of NLRP3 gene and A20 gene. The plasmids were diluted in transfection reagent (18668-11-2, Entranster™-in vivo, Engreen, Beijing, China) and intravenously injected into mice, 5 μg plasmids per mouse, once every 7 days, according to previous study[30,31]. The aortas were harvested on the 90th day after the first plasmid injection.

Transfection in ECs and VSMCs was preformed using the electroporation method. Plasmids were diluted in the electroporation specific reagent (98,668–20, Entranster™-E, Engreen, Beijing, China). ECs (10^5) and VSMC (10^5) were treated with 4 μg plasmid and received once electric shock at 120 V and 150 V respectively, using a gene introduction instrument (SCIENTZ-2C, Scientz, Ningbo, China). After 36 h of electroporation transfection, cells were switched to fresh LG or HG culture medium and treated with STS (100 μM[32], S107694, ALADDIN, Shanghai, China). Change the fresh culture medium containing STS in LG and HG every 24 h. Changes

in inflammasome activation and cellular senescence-related markers were assessed at the 108th hour after electroporation transfection.

Immunofluorescence analysis

Diabetic mice were treated with STS (intravenously injection 10 mg/kg/day[33], S107694, Aladdin, Shanghai, China), PEG-CAT (intravenously injection, 1000U/48 h, C4963-2MG, Sigma, USA) for 90 days. After treatment, the mice were sacrificed, and their aortas were collected and removed adventitia. The aortas fixed by 4% paraformaldehyde (PFA) were cut at 5 μm by a pathological microtome (KD2260, KEDI, Zhejiang, China). The sections were blocked by a blocking solution (P0220, Beyotime, Shanghai, China) after antigen retrieval (using Sodium citrate buffer). The sections were incubated with the primary antibody mouse anti-Waf1/Cip1/CDKN1A p21 antibody (1:100, sc-6246, Santa Cruz, USA), mouse anti-NLRP3 (1:100, 68102-1-Ig, Proteintech, Wuhan, China), rabbit anti-PYCARD (ASC, 1:100, CY5689, Abways, Shanghai, China) overnight at 4 °C, and the second fluorescent antibody Goat Anti-Mouse IgG (H + L) Alexa Fluor 594 (1:200, AB0152, Abways, Shanghai, China), Goat Anti-Rabbit IgG (H + L) Alexa Fluor 488 (1:200, AB0141, Abways, Shanghai, China), 4',6-diamidino-2-phenylindole (DAPI) (C1006, Beyotime, Shanghai. China) labeled nuclei. Images were photographed by a fluorescent microscope (FRD-6C, Cossim, Beijing, China). The integrated density of immunofluorescence was calculated by Image J software (NIH, Littleton, CO, USA).

ECs and VSMCs (5×10^4 cells) were seeded in 35 mm diameter confocal dishes. After treatment with LG, HG, STS (100 μM), PEG-CAT (200U/ml, C4963-2MG, Sigma, USA), BAY11-7082 (1 μM, HY13453, MCE, Shanghai, China), a specific nuclear factor kappa B (NFκB) pathway inhibitor[34], cells were washed three times by PBS (137 mM NaCl, 2.7 mM KCl, 10 mM Na_2HPO_4, 1.8 mM KH_2PO_4) and fixed by 4% PFA for 30 min. Cell membrane was perforated by 0.3% Triton X-100 (BS084, Biosharp, Hefei, China) for 15 min and cells were blocked with blocking solution (P0220, Beyotime, Shanghai, China) for 15 min. Then cells were incubated with the primary antibodies, mouse anti-NLRP3 (1:100, 68,102–1-Ig, Proteintech, Wuhan, China) and rabbit anti-PYCARD (ASC, 1:100, CY5689, Abways, Shanghai, China), mouse anti-Waf1/Cip1/CDKN1A p21 antibody (1:100, sc-6246, Santa Cruz, Shanghai, China), overnight at 4 °C, and the second fluorescent antibody Goat Anti-Mouse IgG (H + L) Alexa Fluor 594 (1:200, AB0152, Abways, Shanghai, China), Goat Anti-Rabbit IgG (H + L) Alexa Fluor 488 (1:200, AB0142, Abways, Shanghai, China), 2 h at room temperature. DAPI (C1006, Beyotime, Shanghai. China) labeled nuclei. Fluorescent images were photographed and processed as the procedure of vascular sections.

Immunohistochemistry (IHC)

IHC in aortas was performed according to our previous study[29]. After deparaffinization and rehydration, aorta sections were blocked with 3% hydrogen peroxide (PH1884, Phygene, Fuzhou, China) at room temperature for 10 min after antigen retrieval (using Sodium citrate buffer). Sections were blocked with blocking solution (P0220, Beyotime, Shanghai, China) for 10 min. The primary antibodies rabbit anti-catalase (1:100, CY6783, Abways, Shanghai, China) was applied for 12 h at 4 °C, followed by the incubation with horseradish peroxidase-conjugated rabbit anti-goat IgG (1:500, AB0101, Abways, Shanghai, China) for 1 h at room temperature. 3, 3-Diaminobenzidine (DAB, PH0728, Phygene, Fuzhou, China) was used to develop the positive area in aortas. Sections were counter-stained with hematoxylin, and the images were captured using a microscope (FRD-6C, Cossim, Beijing, China). The percent of CAT positive area was determined by Image J software with the IHC image analysis toolbox (NIH, Littleton, CO, USA).

ECs and VSMCs (5×10^4 cells) were seeded in 35 mm diameter confocal dishes. After treatment, fixed the cells with pre-cooled anhydrous ethanol for 30 min, then block with 1% hydrogen peroxide solution for 10 min. Next, incubate with the primary antibody, mouse anti-Waf1/Cip1/CDKN1A p21 antibody (1:100, sc-6246, Santa Cruz, Shanghai, China), overnight at 4 °C. Use DAB for color development, and perform imaging and data processing as with tissue sections.

Hydrogen peroxide detection

The accumulation of hydrogen peroxide in aortas, ECs and VSMCs was detected by the ROSgreen (5 μM in cell experiments, MX5202, Maokangbio, Shanghai, China) staining, a specific hydrogen peroxide probe[35,36]. The ROSgreen was dissolved in DMSO firstly, and diluted with HEPES solution (C0215, Beyotime, Shanghai, China). The mice were intravenously injected with a dilution of ROSgreen (20 μM) and were sacrificed after 1 h. The aortas were then removed, peeled off the adventitia, and then detected the ROSgreen fluorescence using an operating microscope with a fluorescence system (MSD540T, Murzider, Dongguan, China). ECs and VSMCs were treated with a dilution of ROSgreen (5 μM) and were incubated for 20 min. The cells were washed, fixed and detected the ROSgreen fluorescence. The integrated density of ROSgreen-fluorescence was calculated using Image J software (NIH, Littleton, CO, USA).

Senescence-associated β-galactosidase (SA-β-gal) staining

Accumulation of SA-β-gal was detected using a commercial kit (C0602, Beyotime, Shanghai, China). Aortas without adventitia, ECs and VSMCs were fixed immediately after treatment, washed by PBS three times, and stained in SA-β-gal staining solution. Aortas and cells photographs were taken by an operating microscope (MSD540T, Murzider, Dongguan, China) and an inverted microscope (FRD-6C, Cossim, Beijing, China) respectively. The area of SA-β-gal staining (green staining) was calculated using the Image J software (NIH, Littleton, CO, USA).

Masson staining

The collagen accumulation in aortas without adventitia was measured using the Masson staining kit (WLA045a, Wanleibio, Shenyang, China). After deparaffinization, the sections of aorta were hydrated using gradient concentration ethanol. The hydrated sections were then stained with cytoplasmic staining solution (red) for 10 min, after rinsing once with distilled water, treat with differentiation solution for 1 min. Then the sections were stained with collagen staining solution (blue) for 1 min. The stained sections were dehydrated using gradient concentration ethanol, and covered by neutral balsam and coverslips. The photographs of sections were taken by an inverted microscope (FRD-6C, Cossim, Beijing, China). The area of collagen staining (blue staining) was calculated using the Image J software (NIH, Littleton, CO, USA). The freehand selection tool in ImageJ was used to precisely select the blue-stained areas on the vessel wall and measured their area as area 1. Then, the freehand selection tool was used again to select the entire vessel wall and measured its area as area 2. The percentage of collagen deposition area (blue-stained) was calculated by using the formula (area 1/area 2) × 100%.

Western blot analysis

Western blot analysis was performed as described previously[29]. Briefly, cell total protein samples were extracted using Protein Extraction Kit (P0033, Beyotime, Shanghai, China), the mice vascular protein samples were extracted using mammalian active protein extraction kit (P0013M, Beyotime, Shanghai, China). Protein concentration was quantified by using a BCA Protein Assay Kit (P0010, Beyotime, Shanghai, China). According to the quantification, protein samples were adjusted to equal with 5 × loading buffer (P0015, Beyotime, Shanghai, China), and samples were boiled for 5 min at 95 °C. Equal amounts of cell lysate protein were resolved by SDS-PAGE using 5% (w/v) stacking and 7.5–12% (w/v) separating polyacrylamide gels. The gels were cut based on the molecular weight of the target proteins, and then transferred to 0.22 μm nitrocellulose filter membrane (NC, P-N66485 PALL, Beijing, China), which were then blocked for 1.5 h in 5% (w/v) non-fat milk diluted in Tris-buffered saline (TBS, 100 mM Tris–HCL, pH 7.4) with 0.01% (v/v) Tween-20, and incubated with the primary antibodies overnight at 4 °C. The primary antibodies used were rabbit anti-A20/TNFAIP3 (1:500, WL00820, Wanleibio, Shenyang, China), mouse anti-NLRP3 (1:1000, 68102-1-Ig, Proteintech, Wuhan, China), rabbit anti-Phospho-NLRP3 (Ser194) (1:500, AF3555, Affinity, Changzhou, China), rabbit anti-catalase (1:1000, CY6783, Abways, Shanghai, China), rabbit anti-α-tubulin (1:4000, Abways, AB0048, Shanghai, China), rabbit anti-NFκB (p65, 1:500, WL01273b, Wanleibio, Shenyang, China), rabbit anti-p-NFκB (p-p65, 1:500, WL02169, Wanleibio, Shenyang, China), rabbit anti-IκBα (1:500, WL01936, Wanleibio, Shenyang, China), and rabbit anti-p-IκBα (1:500, WL02495, Wanleibio, Shenyang, China). After being washed for three times, the membranes were incubated with Goat anti-Rabbit IgG (H + L) HRP (1:4000, AB0101, Abways, Shanghai, China), Goat anti-mouse IgG (H + L) HRP (1:4000, AB0102, Abways, Shanghai, China) for 1.5 h. The blot was detected by an automatic chemiluminescence/muti-color fluorescence image analysis system (Champ Chemi 610, Sagecreation, Beijing, China) with electrochemiluminescence (ECL, BMU102-CN, Abbkine, Wuhan, China). Densitometric analysis of the images was performed with Image J software (NIH, Littleton, CO, USA).

Vascular tension recording

The contraction and relaxation functions of aortas was detected by tension detection system (BL-420S, TaiMeng, Chengdu, China) as described previously[21,29]. Mice were anaesthetized and aortas were quickly removed and immersed into Krebs Henseleit solution (mM) (KH, pH 7.4, 119.0 NaCl, 25.0 $NaHCO_3$, 11.1 Glucose, 2.4 $CaCl_2$, 4.7 KCl, 1.2 KH_2PO_4, 1.2 $MgSO_4$, 0.024 Na_2EDTA). Aortas were carefully dissected into a transparent tube, and then cut into vascular rings with a width of approximately 3 mm. The endothelium of aortas was removed using a flexible wire (0.38 mm diameter) or retained. The vascular rings were then suspended in a water-jacketed tissue bath and the tension tested. KH solution was maintained at 37 °C and the mixed gas containing 95% O_2, and 5% CO_2 was continuously bubbled through the bath. When the tension of the rings stabilized at the basal level, the aortic rings were contracted with phenylephrine (Phe, 1 μM, P106007, Aladdin, Shanghai, China) to obtain a pre-constriction response, the rings were then assessed for endothelium dependent relaxation (acetylcholine, Ach, Ach induces endothelial cells to produce nitric oxide and other vasodilators, causing the smooth muscle layer to relax.) (Ach, 1×10^{-9}–10^{-5} M, A111014, Aladdin, Shanghai, China) and sodium nitroprusside (SNP, 1×10^{-9}–10^{-5} M, S305727, Aladdin, Shanghai, China, SNP directly provides exogenous nitric oxide, directly causing the vascular smooth muscle layer to relax.) induced relaxation, and the record of relaxation induced by Ach (1×10^{-4} M), SNP (1×10^{-4} M) in the Ctrl group was set as 100% response to the Ach or SNP.

Detection of active caspase-1, IL-1β, IL-18 levels

Caspase-1 activity was assessed using a commercially available Caspase-1 Activity Assay Kit (C1101, Beyotime, Shanghai, China), following previously established protocols[37]. Active levels of IL-1β and IL-18 were determined using commercial ELISA kits (SEKM-0002, SEKM-0019, Solarbio, Beijing, China).

Arterial homogenate, EC and VSMC lysate were centrifuged at 15,000 rpm/min for 15 min at 4 °C. The supernatants were collected and qualified by a BCA assay kit (P0010, Beyotime, Shanghai, China). Caspase-1 activity in an equal amount of protein, approximately 200 μg, was determined immediately. Ac-YVAD-pNA was added to the supernatant and incubated for 60–120 min at 37 °C. When the solution exhibited a distinct yellow color, the samples were measured using a microplate reader (Thermo Fisher Scientific, USA) at 405 nm. The detection of IL-1β and IL-18 was performed according to kit specification, and the optical density (OD) was measured at 450 nm.

Statistics

Statistical analysis was performed with Prism 9.0 (GraphPad Software). Data are presented as means ± SEM. Significant differences between and within multiple groups were examined using ANOVA for repeated measures, followed by Duncan's multiple-range test. The Independent-Samples t-test was used to detect significant differences between two groups. $P < 0.05$ was considered statistically significant.

Ethics approval and consent to participate

Animal handling and experimental procedures were approved by the Ethics Committee of Changzhi Medical College (DW2022053), following the guidelines of the US National Institutes of Health and the Animal Research Reporting In Vivo Experiments (ARRIVE).

Results

STS alleviates senescence in diabetic aortas and HG-treated ECs and VSMCs

We evaluated random blood glucose (RBG) level and oral glucose tolerance test (OGTT) changes in both control and diabetic mice with or without STS treatment. We found that STS intervention did not significantly affect blood glucose and glucose tolerance test results in both control and diabetic mice (Supplemental Fig. 1A,B). These results suggest that STS does not exert a direct impact on blood glucose levels in diabetic mice.

In the aortas of diabetic mice, we evaluated the catalase (CAT) level, hydrogen peroxide accumulation, p21 expression as a marker of cell senescence, as well as the areas of SA-β-gal staining and collagen deposition, along with the assessment of relaxant function. Our results showed a decrease in the positive area of CAT (Fig. 1A,B). The integrated density of ROSgreen fluorescence (Fig. 1C,D) and p21 immunofluorescence (Fig. 1E,F) were enhanced. The area of SA-β-gal staining (Fig. 1G,H) and collagen deposition (Fig. 1I,J) were also increased. Additionally, Ach and SNP-induced vascular relaxation deteriorated (Fig. 1K,L) in diabetic mice aortas. STS treatment partially reversed these changes (Fig. 1A–L).

These results indicate that STS protects CAT, reduces hydrogen peroxide accumulation, alleviates senescence and relaxant function in diabetic blood vessels.

The endothelium and the smooth muscle layer are the main structural constituents of blood vessels. Therefore, we detected the senescent marker in ECs and VSMCs under HG culture. We found a decrease in the expression of A20 (a NFκB inhibitor) and CAT in ECs and VSMCs treated with HG (Fig. 1M–P). This decrease was restored by STS treatment. Meanwhile, treatment with HG resulted in an increase in the p21 positive area (Fig. 1Q,R,U,V), ROSgreen fluorescence (Fig. 1Q,S,U,W), and the area of SA-β-gal staining (Fig. 1Q,T,U,X) in ECs and VSMCs. STS treatment partially prevented these changes in ECs and VSMCs (Fig. 1Q–X).

Additionally, similar to PEG-CAT intervention, STS inhibits vascular wall p21 expression (Supplemental Fig. 2A,B). It also suppresses the integrated density of ROSgreen and the SA-β-gal staining area (Supplemental Fig. 2C–H) in both ECs and VSMCs.

These results suggest that hyperglycemic conditions, a major characteristic of diabetes, lead to a decrease in the level of CAT, the accumulation of hydrogen peroxide, senescence, and loss of relaxant function. STS alleviates senescence and ROS generation by protecting the level of CAT in both ECs and VSMCs treated with HG. The mechanism of STS protection may be related to the recovery of A20.

STS inhibits the activation of NLRP3 inflammasome in diabetic aortas, HG-treated ECs and VSMCs

A study has shown that inhibition of NLRP3 inflammasome synchronized CAT recovery[38]. We inferred that the suppression of oxidative stress and senescence by STS was associated with the inhibition of NLRP3 inflammasome. Therefore, we detected the activation of the NLRP3 inflammasome in diabetic blood vessels, HG-treated ECs and VSMCs.

We found that the immunofluorescence colocalization of NLRP3 (red) and ASC (green, a bridging adaptor protein of inflammasome) increased in diabetic blood vessels. The merged dots (yellow) also showed an increase (Fig. 2A,B). Meanwhile, the production of NLRP3 dimer, the expression of NLRP3, and the phosphorylation of NLRP3 at the serine 194 site were induced (Fig. 2C,D). Additionally, the active caspase-1 (also known as the IL-1 converting enzyme), mature IL-1β, and IL-18 were produced in diabetic blood vessels (Fig. 2E–G). STS treatment inhibited these changes (Fig. 2A–G).

We further observed the activation of the NLRP3 inflammasome in HG-treated ECs and VSMCs. Similar to the results in the vascular wall, HG culture induced the production of NLRP3 dimer, the expression of NLRP3, and the phosphorylation of NLRP3 at the serine 194 site in ECs and VSMCs (Fig. 2H,I,O,P). Moreover, the active caspase-1, mature IL-1β, and IL-18 were increased in HG-treated ECs and VSMCs (Fig. 2J–L,Q–S). HG treatment also increased the immunofluorescence colocalization of NLRP3 (red), ASC (green), and their merged dots (yellow) in ECs and VSMCs (Fig. 2M,N,T,U). STS treatment inhibited these changes as well (Fig. 2H–U).

These results indicate that the diabetic pathological environment induces the activation of the NLRP3 inflammasome in blood vessels. STS limits the activation of the NLRP3 inflammasome by inhibiting the production of the NLRP3 dimer, the expression of NLRP3, the phosphorylation of NLRP3 at the serine 194 site, and the assembly of NLRP3 and ASC in diabetic aortas, and in HG-treated ECs and VSMCs.

STS alleviates vascular senescence by inhibiting the NLRP3 inflammasome under diabetic condition

To explore the correlation between the senescence alleviation of STS and the inhibition of NLRP3 inflammasome, we transfected diabetic mice, HG-treated ECs and VSMCs with NLRP3-activated plasmid (NLRP3 over-expression, NOE) and NLRP3-knockout (NKO) plasmid. In the pre-experiment, we evaluated the transfection effect

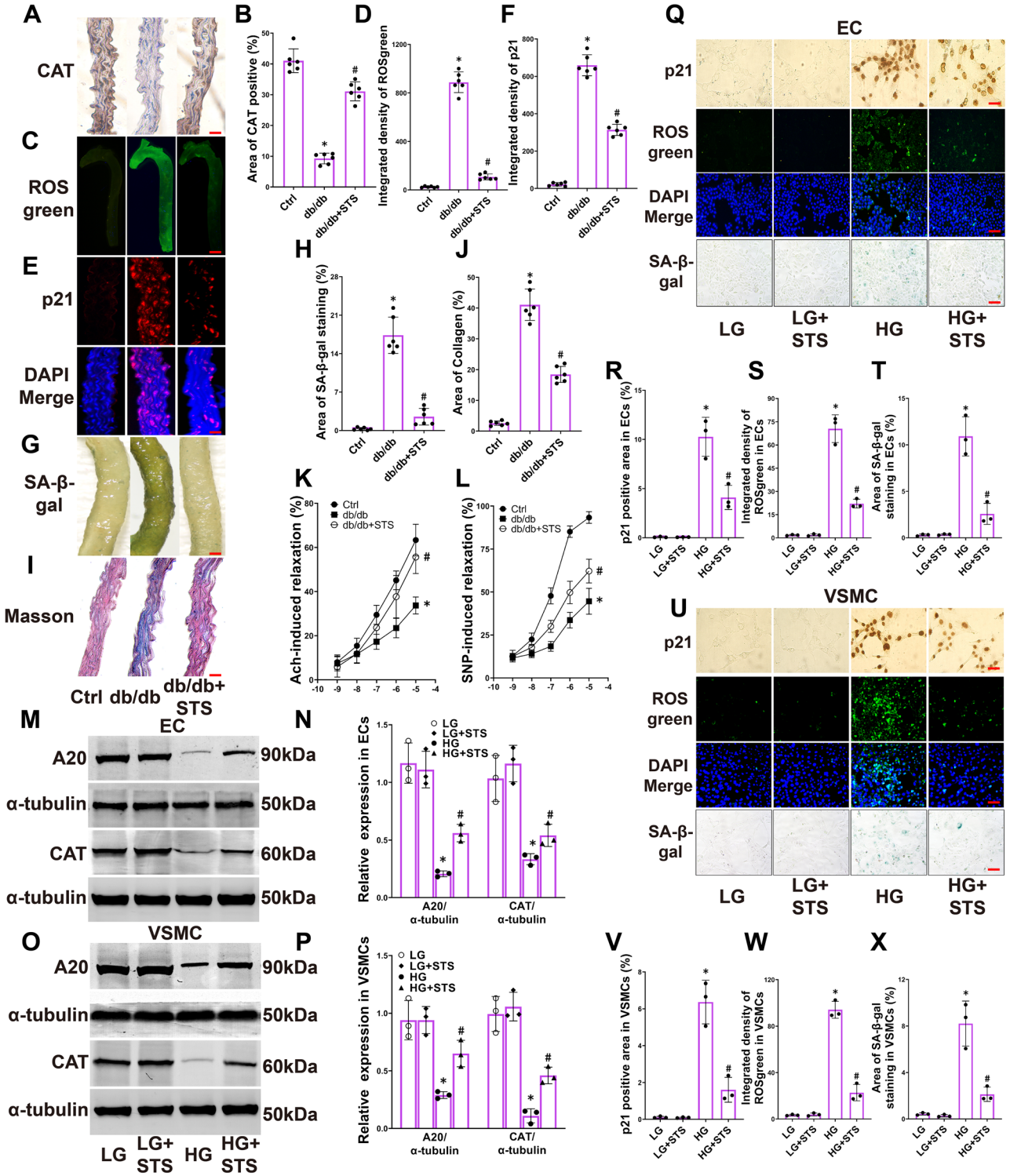

Figure 1. STS alleviates senescence in diabetic aortas and HG-treated ECs and VSMCs. (**A**–**J**) Representative images and the summarized data of CAT (400×, scale bar: 20 μm), ROSgreen staining fluorescence (15×, scale bar: 1000 μm), p21 immunofluorescence (400×, scale bar: 20 μm), SA-β-gal staining (40×, scale bar: 200 μm), Masson staining (400×, scale bar: 20 μm) in aortas; (**K**,**L**) The summarized data of aortas responding to Ach and SNP; The ECs and VSMCs were treated with low glucose (5 mM, LG) or high glucose (30 mM, HG) for 72 h, with or without STS (100 μM) treatment. (**M**–**P**) Representative Western blot gels and the summarized data of show the protein expression of A20, CAT in ECs and VSMCs; (**Q**) and (**U**) Representative images of p21 IHC (400×, scale bar: 20 μm), ROSgreen staining (400×, scale bar: 20 μm) and SA-β-gal staining (400×, scale bar: 40 μm) in ECs and VSMCs; (**R**–**T**) and (**V**–**X**) The summarized data of show p21 positive area, integrated fluorescent density of ROSgreenin and the area of SA-β-gal positive in ECs and VSMCs. $^{*}P<0.05$ vs. Control (Ctrl) or LG; $^{\#}P<0.05$ vs. db/db or HG group (n = 6 in mice, n = 3 in cells). In the aorta results Ctrl represents littermate (wild-type, WT) of db/db mice with no treatment. In the cellular results, STS showed no significant impact on senescence-related markers in the LG group cells. In our animal pre-experiment, we found that STS had no significant effect on CAT and p21 levels in the aorta of Ctrl (WT) animals (Supplemental Fig. 3A–D). Therefore, in the animal results, we did not include the intervention of STS in the Ctrl group.

of normal and diabetic animals' aortas, as well as in ECs and VSMCs treated with LG or HG. Our results showed that empty vectors (null-ACT and null-KO) do not exert significant regulatory effects on the expression levels of NLRP3 in aortas, ECs and VSMCs (Supplemental Figs. 4A,B, 5A,B, 6A,B). Within 10 days plasmid injection via the tail vein, the expression of NLRP3 in the aortas was significantly increased or inhibited (Supplemental Fig. 4C–F). Additionally, 36 to 120 h after electroporation, the expression of NLRP3 in ECs and VSMCs was significantly increased or inhibited (Supplemental Figs. 5C–F, 6C–F). The results showed successful regulation of NLRP3 expression levels in both aortas and cells.

We discovered that NKO plasmid transfection preserved the level of CAT in diabetic aortas (Fig. 3A,B). It also inhibited the expression of p21 (Fig. 3C,D), reduced the area of SA-β-gal staining (Fig. 3E,F), and decreased collagen deposition (Fig. 3G,H). Additionally, the NKO plasmid maintained Ach and SNP induced relaxation of diabetic blood vessels (Fig. 3I,J). STS treatment had similar effects (Fig. 3A–J). However, these effects of STS were cancelled by treatment with NOE plasmid (Fig. 3A–J).

We verified these results in ECs and VSMCs. We found that the effects of STS on restoring CAT levels (Fig. 3K–N), and limiting ROSgreen fluorescence (Fig. 3O,P,R,S) and the area of SA-β-gal staining (Fig. 3O,Q,R,T) were nullified by treatment with NOE plasmid in HG-treated ECs and VSMCs. Both NKO plasmid and STS treatment had similar effects on alleviating these markers (Fig. 3K–T).

These results suggest that STS alleviates vascular oxidative stress and senescence by inhibiting the NLRP3 inflammasome to protect the CAT level under diabetic condition.

STS suppresses the expression of NLRP3 and senescence by inhibiting of NFκB pathway in HG-treated ECs and VSMCs

To investigate the mechanism by which STS inhibits the NLRP3 inflammasome activation, we used the NFκB inhibitor BAY11-7082 (BAY) to block the NFκB pathway in HG-treated ECs and VSMCs. We observed that BAY inhibited the phosphorylation of IκBα (Fig. 4A,B,E,F) and p65 (Fig. 4A,C,E,G). It also suppressed the expression of NLRP3 (Fig. 4A,D,E,H) and p21 immunofluorescence (Fig. 4I,J,L,M). Additionally, BAY decreased the area of SA-β-gal staining (Fig. 4I,K,L,N). STS had similar effects on these changes (Fig. 4A–N).

These results indicate that STS inhibits the expression of NLRP3 and senescence by inactivating the NFκB pathway in ECs and VSMCs treated with HG.

STS suppresses the activation of NLRP3 inflammasome and vascular senescence by activating A20 under diabetic condition

A20, also known as Tumor Necrosis Factor (TNF) alpha-induced protein 3 (TNFAIP3), was discovered as a primary response gene in human ECs stimulated with TNF, acting as a negative feedback regulator that inhibits cell death by repressing the TNFα-NFκB pathway[39]. Its inhibitory effect on NFκB signaling is mediated through interference with the ubiquitination status of multiple NFκB signaling proteins[39]. The relationship between the A20 pathway and vascular cell senescence requires further investigation.

To explore the relationship between the alleviation of senescence by STS and the expression of A20, we transfected diabetic blood vessels, HG-treated ECs and VSMCs with A20-knockout (AKO) plasmid and A20-activated (A20 over-expression, AOE) plasmid. In the pre-experiment, we evaluated the transfection effect of normal and diabetic animals' aortas, as well as in ECs and VSMCs treated with LG or HG. Our results showed that empty vectors (null-ACT and null-KO) do not exert significant regulatory effects on the expression levels of A20 in aortas, ECs and VSMCs (Supplemental Figs. 7A,B, 8A,B, 9A,B). Within 10 days after plasmid injection via the tail vein, the expression of A20 in the aortas was significantly increased or inhibited (Supplemental Fig. 7C–F). Additionally, 36 to 120 h after electroporation, the expression of A20 in ECs and VSMCs was significantly increased or inhibited (Supplemental Figs. 8C–F, 9C–F). These results confirmed successful regulation of A20 expression levels in both animals and cells.

We found that the AOE plasmid limited the expression of NLRP3 (Fig. 5A,B) and maintained the level of CAT (Fig. 5C,D). It inhibited the integrated density of p21 immunofluorescence (Fig. 5E,F), reduced the area of SA-β-gal staining (Fig. 5G,H), and decreased collagen deposition (Fig. 5I,J). Additionally, the AOE plasmid preserved Ach and SNP induced vascular relaxation in diabetic blood vessels (Fig. 5K,L). STS treatment had similar effects (Fig. 5A–L). However, these effects of STS were eliminated by treatment with the AKO plasmid (Fig. 5A–L).

We confirmed these results in ECs and VSMCs treated with HG. We found that the effects of STS on inhibiting NLRP3 phosphorylation, NLRP3 dimer production, and p65 phosphorylation, as well as restoring the expression of CAT (Fig. 5M–P), were dismissed by treatment with the AKO plasmid in HG-treated ECs and VSMCs. STS also suppressed the active caspase-1 (Fig. 5Q,R) and limited the area of SA-β-gal staining (Fig. 5S,V). The AOE plasmid and STS treatment had similar effects on alleviating these markers (Fig. 5M–V).

These results suggest that STS alleviates vascular senescence by activating A20 to inhibit the NFκB and NLRP3 pathway under diabetic condition.

Discussion

The present study demonstrated that STS sustained CAT level, reduced the accumulation of hydrogen peroxide in ECs and VSMCs by stimulating A20 expression and inhibiting the NFκB-NLRP3 inflammasome pathway, thereby alleviating vascular senescence in diabetic mice. Additionally, under hyperglycemic conditions, the present study revealed both phosphorylation at the serine 194 site of NLRP3 and the formation of NLRP3 dimers, collectively contributing to the potential foundation for NLRP3 inflammasome activation. This study also substantiated that STS mitigated senescence of ECs and VSMCs in the HG environment.

It has been confirmed that tanshinone IIA protects ECs function and inhibits VSMCs proliferation and migration by inhibiting oxidative stress and inflammatory pathways[28,40]. However, the effects of tanshinone IIA

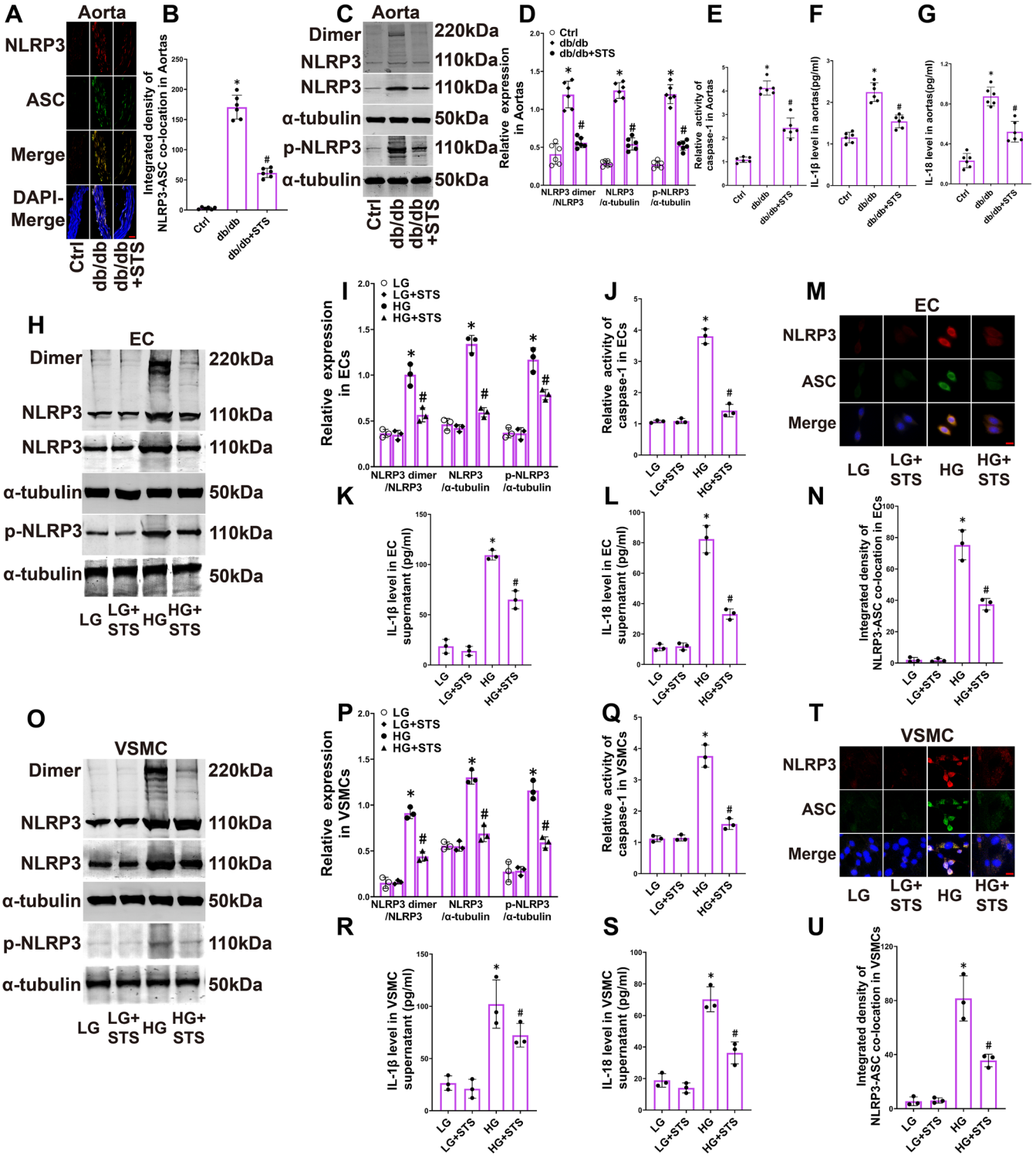
A
Aorta
NLRP3
ASC
Merge
DAPI-Merge
Ctrl
db/db
db/db +STS
B
Integrated density of NLRP3-ASC co-location in Aortas
Ctrl
db/db
db/db+STS
C
Aorta
Dimer
NLRP3
NLRP3
α-tubulin
p-NLRP3
α-tubulin
220kDa
110kDa
110kDa
50kDa
110kDa
50kDa
Ctrl
db/db
db/db +STS
D
Ctrl
db/db
db/db+STS
Relative expression in Aortas
NLRP3 dimer /NLRP3
NLRP3 /α-tubulin
p-NLRP3 /α-tubulin
E
Relative activity of caspase-1 in Aortas
F
IL-1β level in aortas(pg/ml)
G
IL-18 level in aortas(pg/ml)
H
EC
Dimer
NLRP3
NLRP3
α-tubulin
p-NLRP3
α-tubulin
220kDa
110kDa
110kDa
50kDa
110kDa
50kDa
LG
LG+ STS
HG
HG+ STS
I
LG
LG+STS
HG
HG+STS
Relative expression in ECs
NLRP3 dimer /NLRP3
NLRP3 /α-tubulin
p-NLRP3 /α-tubulin
J
Relative activity of caspase-1 in ECs
K
IL-1β level in EC supernatant (pg/ml)
L
IL-18 level in EC supernatant (pg/ml)
M
EC
NLRP3
ASC
Merge
LG
LG+ STS
HG
HG+ STS
N
Integrated density of NLRP3-ASC co-location in ECs
O
VSMC
Dimer
NLRP3
NLRP3
α-tubulin
p-NLRP3
α-tubulin
220kDa
110kDa
110kDa
50kDa
110kDa
50kDa
LG
LG+ STS
HG
HG+ STS
P
LG
LG+STS
HG
HG+STS
Relative expression in VSMCs
NLRP3 dimer /NLRP3
NLRP3 /α-tubulin
p-NLRP3 /α-tubulin
Q
Relative activity of caspase-1 in VSMCs
R
IL-1β level in VSMC supernatant (pg/ml)
S
IL-18 level in VSMC supernatant (pg/ml)
T
VSMC
NLRP3
ASC
Merge
LG
LG+ STS
HG
HG+ STS
U
Integrated density of NLRP3-ASC co-location in VSMCs

◂**Figure 2.** STS inhibits the activation of NLRP3 inflammasome in diabetic aortas, HG-treated ECs and VSMCs. (**A**,**B**) Representative immunofluorescence images (400×, scale bar: 20 μm) and summarized integrated density of NLRP3 and ASC colocalization in aortas; (**C**,**D**) Representative Western blot gels and summarized data show the production of NLRP3 dimer, the expression of NLRP3, the phosphorylation of NLRP3 at serine 194 site in aortas; (**E**–**G**) The summarized data show active caspase-1, mature IL-1β and IL-18 in aortas; (**H**,**I**) Representative Western blot gels and summarized data show the production of NLRP3 dimer, the expression of NLRP3, the phosphorylation of NLRP3 at serine 194 site in ECs; (**J**–**L**) The summarized data show the active caspase-1, mature IL-1β and IL-18 in ECs; (**M**,**N**) Representative immunofluorescence images (800×, scale bar: 10 μm) and summarized integrated density of NLRP3 and ASC colocalization in ECs; (**O**,**P**) Representative Western blot gels and summarized data show the production of NLRP3 dimer, the expression of NLRP3, the phosphorylation of NLRP3 at serine 194 site in VSMCs; (**Q**–**S**) The summarized data show the active caspase-1, mature IL-1β and IL-18 in VSMCs; (**T**,**U**) Representative immunofluorescence images (800×, scale bar: 10 μm) and summarized integrated density of NLRP3 and ASC colocalization in VSMCs. $^{*}P<0.05$ vs. Control (Ctrl) or LG; $^{\#}P<0.05$ vs. db/db group or HG (n = 6 in mice, n = 3 in cells). In the cellular results, STS showed no significant impact on NLRP3 inflammasome activation-related markers in the LG treated cells. In our animal pre-experiment, we found that STS had no significant effect on NLRP3-ASC colocalization in the aorta of Ctrl (WT) animals (Supplemental Fig. 3E,F). Therefore, in the animal results, we did not include the intervention of STS in the Ctrl group.

and its sulfonic acid product (STS) on vascular senescence, particularly under diabetic conditions, has not yet been reported. Some studies have shown that downregulating oxidative stress alleviates ECs and VSMCs senescence induced by HG[41–43]. But the mechanism of inhibiting ROS generation is not clear. Previous studies have shown that the expression of catalase (CAT), a key enzyme of anti-oxidase system, was downregulated under HG culture[44,45]. Similar to these conclusions, our results showed that the level of CAT was suppressed by HG, resulting in the accumulation of hydrogen peroxide and vascular senescence; STS treatment alleviated vascular senescence by preserving the CAT level. Furthermore, our results reveled that the protection of CAT by STS was related to the inhibition of the NLRP3 inflammasome.

The activation of NLRP3 inflammasome has been considered closely related to the generation of ROS. Generally, the level of ROS upregulation is one of the key mechanisms of the activation of NLRP3 inflammasome. Studies have suggested that mitochondria damage-induced ROS generation activates the NLRP3 inflammasome, leading to apoptosis of renal tubular epithelial cells and inflammatory reaction in nerve cells[46,47]. Other studies believed that ROS generation induces the loss of nitric oxide in ECs and calcification in VSMCs by activating the NLRP3 inflammasome[16,48]. Our results found that NLRP3 upregulation inhibited the CAT level in ECs and VSMCs treated with HG. This conclusion differs from the conclusions of previous studies. Nevertheless, our results exhibit similarities to certain fragmented findings in the existing literature. Inhibition of the NLRP3 inflammasome activation and restoration of CAT level were observed simultaneously in the research on the treatment of multiple sclerosis[49]. Inhibition of the component proteins required for the assembly of NLRP3 inflammasome and restoration of CAT RNA expression were also observed simultaneously in the research on the treatment of airway epithelial cell injury[50]. What's more, in a study on atherosclerosis treatment, knockout of NLRP3 inhibited ROS generation and protected human aortic endothelial cells[51]. Combining these conclusions, we believe that there is a vicious cycle involving ROS-NLRP3 inflammasome-CAT-ROS in the context of oxidative stress and inflammation. Based on our findings, we hold that this cycle represents a crucial mechanism of cell injury and senescence induced by ROS and the NLRP3 inflammasome. The conclusion is worth further studying.

The exact mechanism of HG-triggered NLRP3 inflammasome activation remains unclear. The post-translational modification (PTM) of NLRP3 protein is considered the basis for the assembly of NLRP3 inflammasome. Recent study have shown that deubiquitination, desumoylation and phosphorylation of NLRP3 play crucial roles in the assembly of NLRP3 inflammasome[52]. More importantly, according to reports, the assembly of the NLRP3 inflammasome may rely on the imperative basic process of NLRP3 oligomerization[53,54]. We found that NLRP3 phosphorylation at serine 194 site and the production of NLRP3 dimer appear to be the vital processes for NLRP3 inflammasome assembly. The NLRP3 phosphorylation result is accorded with the conclusion in previous study[55]. Instead of oligomerization, the HG-induced NLRP3 dimer was observed in our results. We posit that the NLRP3 dimer plays a key role in the activation of the NLRP3 inflammasome. This finding provides a novel PTM clue for high glucose-induced activation of NLRP3 inflammasomes and warrants further investigation.

Studies have shown that tanshinone IIA and STS inhibited the pyroptosis and alleviated the progress of atherosclerosis by suppressing the NLPR3 inflammasome activation in macrophages[56,57]. Additional research has reinforced the idea that STS offers cardiovascular protection by inhibiting the NLRP3 inflammasome. STS inhibited the activation of NLRP3 inflammasome induced by endotoxin and limited myocardial damage[58]. STS also reduced the NLRP3 inflammasome-dependent pyroptosis in ECs, which aided in the mitigation of atherosclerosis progression[59]. In available STS studies, the mechanism for inhibiting the NLRP3 inflammasome is frequently associated with the suppression of the NFκB pathway. However, the manner in which STS hinders the NFκB pathway has received less attention as of yet. According to our results, we believe that STS activates A20, an inhibitor of the NFκB pathway, which then suppresses the phosphorylation and dimerization of NLRP3 protein. This conclusion coincides with studies that have found A20 to inhibit the NLRP3 inflammasome[60,61], and it suggests that the mechanism by which A20 inhibits the NLRP3 inflammasome is associated with the PTM regulation of NLRP3. While study found a downregulation of A20 level in diabetic condition[62], the connection between the NLRP3 inflammasome activation and the loss of A20 in hyperglycemia condition requires further investigation. Our results revealed that A20 expression was inhibited in ECs and VSMCs under HG culture, accompanied by the activation of NFκB pathway and an upregulation of NLRP3 expression. Furthermore, A20

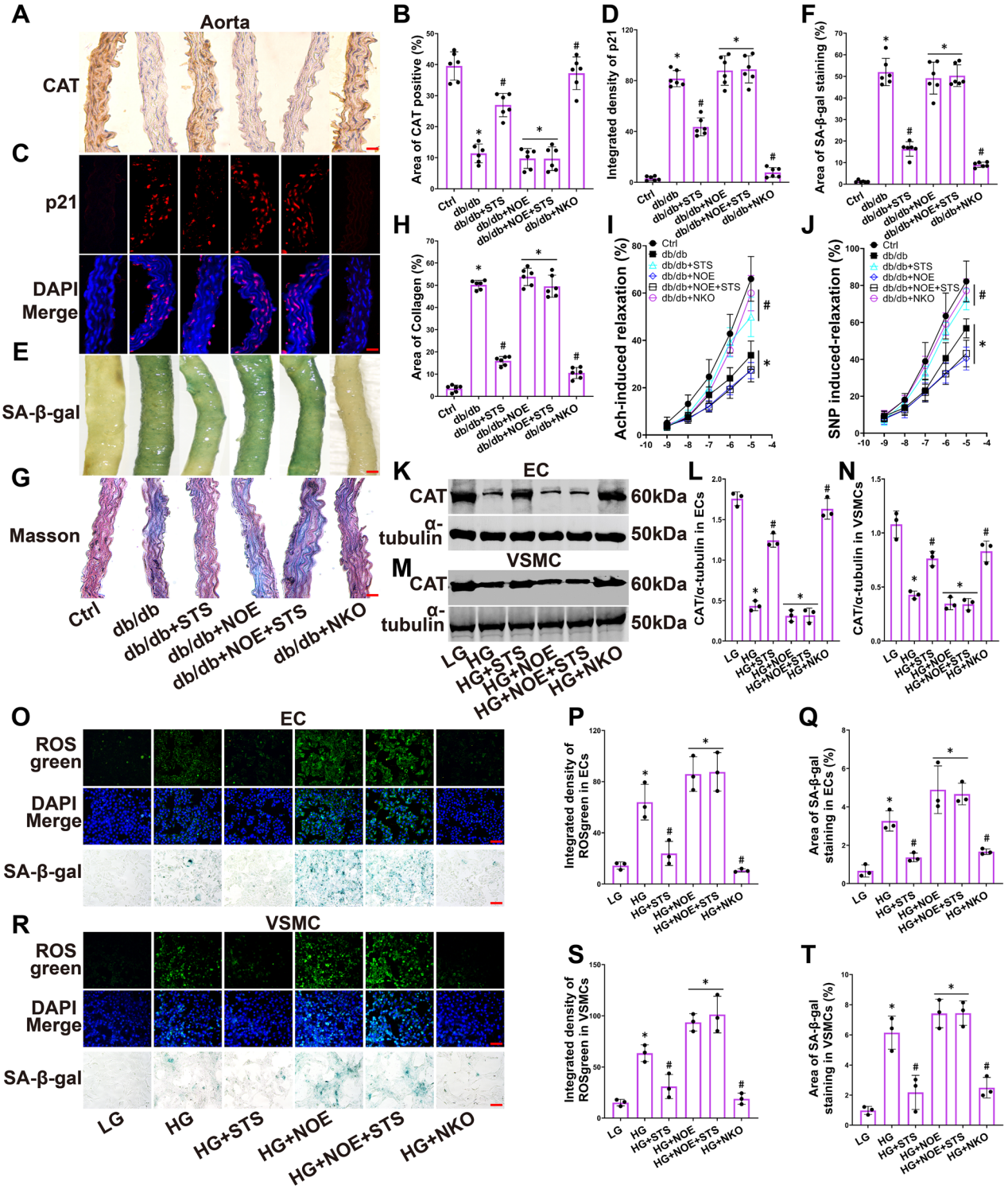

Figure 3. STS alleviates vascular senescence by inhibiting the NLRP3 inflammasome under diabetic condition. (**A**–**H**) Representative images and the summarized data of CAT (400×, scale bar: 20 μm), p21 immunofluorescence (400×, scale bar: 20 μm), SA-β-gal staining (40×, scale bar: 200 μm), Masson staining (400×, scale bar: 20 μm) in aortas; (**I**,**J**) The summarized data of aortas responding to Ach and SNP; (**K**,**L**) and (**M**,**N**) Representative Western blot gels and the summarized data show the expression of CAT in ECs and VSMCs; (**O**–**Q**) and (**R**–**T**) Representative images and the summarized data show the ROGgreen and SA-β-gal staining in ECs and VSMCs. $^{*}P<0.05$ vs. Control (Ctrl) or LG; $^{\#}P<0.05$ vs. db/db or HG group (n = 6 in mice, n = 3 in cells).

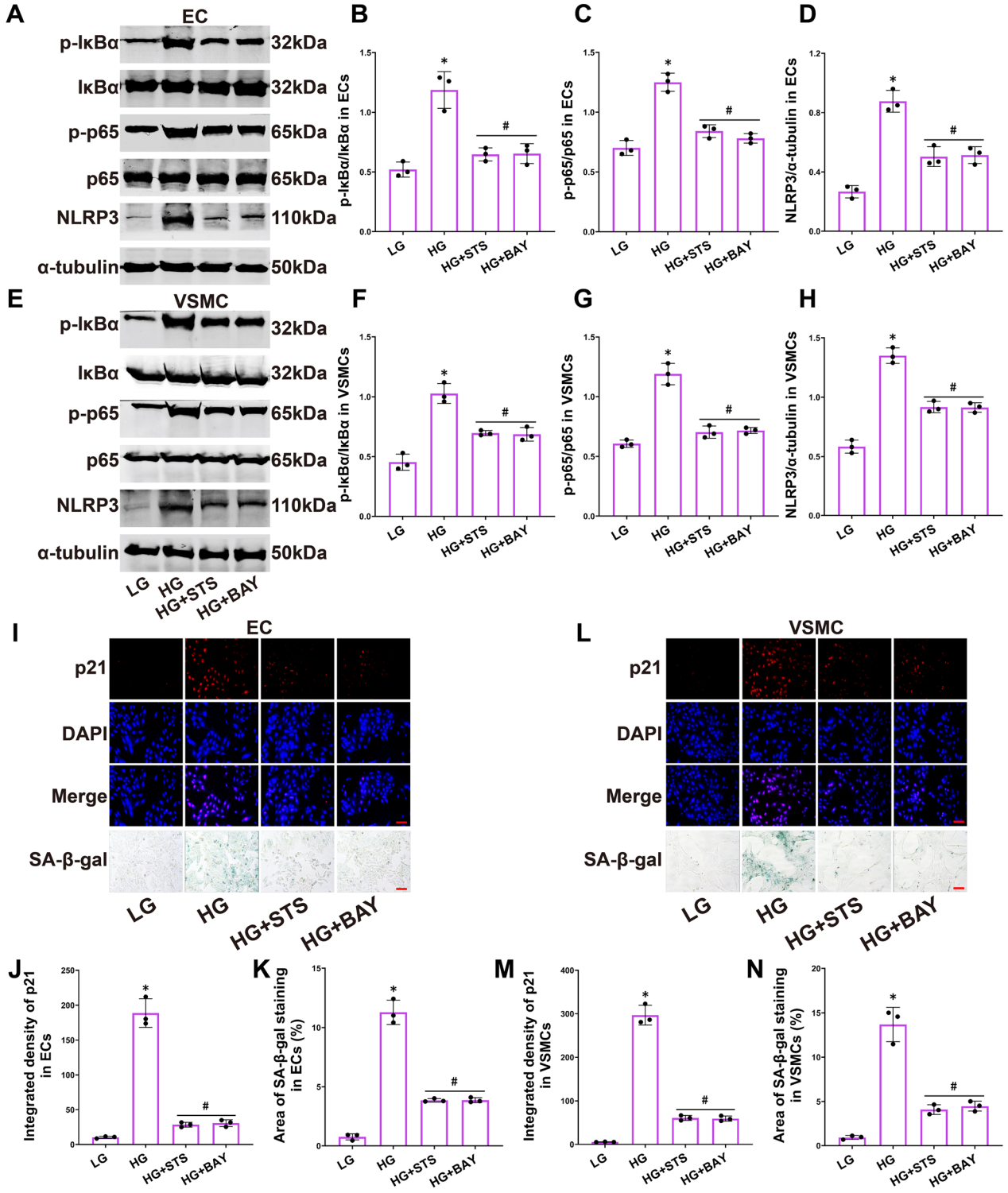

Figure 4. STS suppresses the expression of NLRP3 and senescence by inhibiting of NFκB pathway in HG-treated ECs and VSMCs. (**A**–**D**) Representative Western blot gels and summarized data show the phosphorylation of IκBα and NFκB, and the expression of NLRP3 in ECs; (**E**–**H**) Representative Western blot gels and summarized data show the phosphorylation of IκBα and NFκB, and the expression of NLRP3 in VSMCs; (**I**–**K**) Representative images and the summarized data show p21 immunofluorescence (400×, scale bar: 20 μm) and SA-β-gal staining (400×, scale bar: 20 μm) in ECs; (**L**–**N**) Representative images and the summarized data show p21 immunofluorescence (400×, scale bar: 20 μm) and SA-β-gal staining (400×, scale bar: 20 μm) in VSMCs. $^{*}P<0.05$ vs. LG; $^{\#}P<0.05$ vs. HG treated group (n = 3).

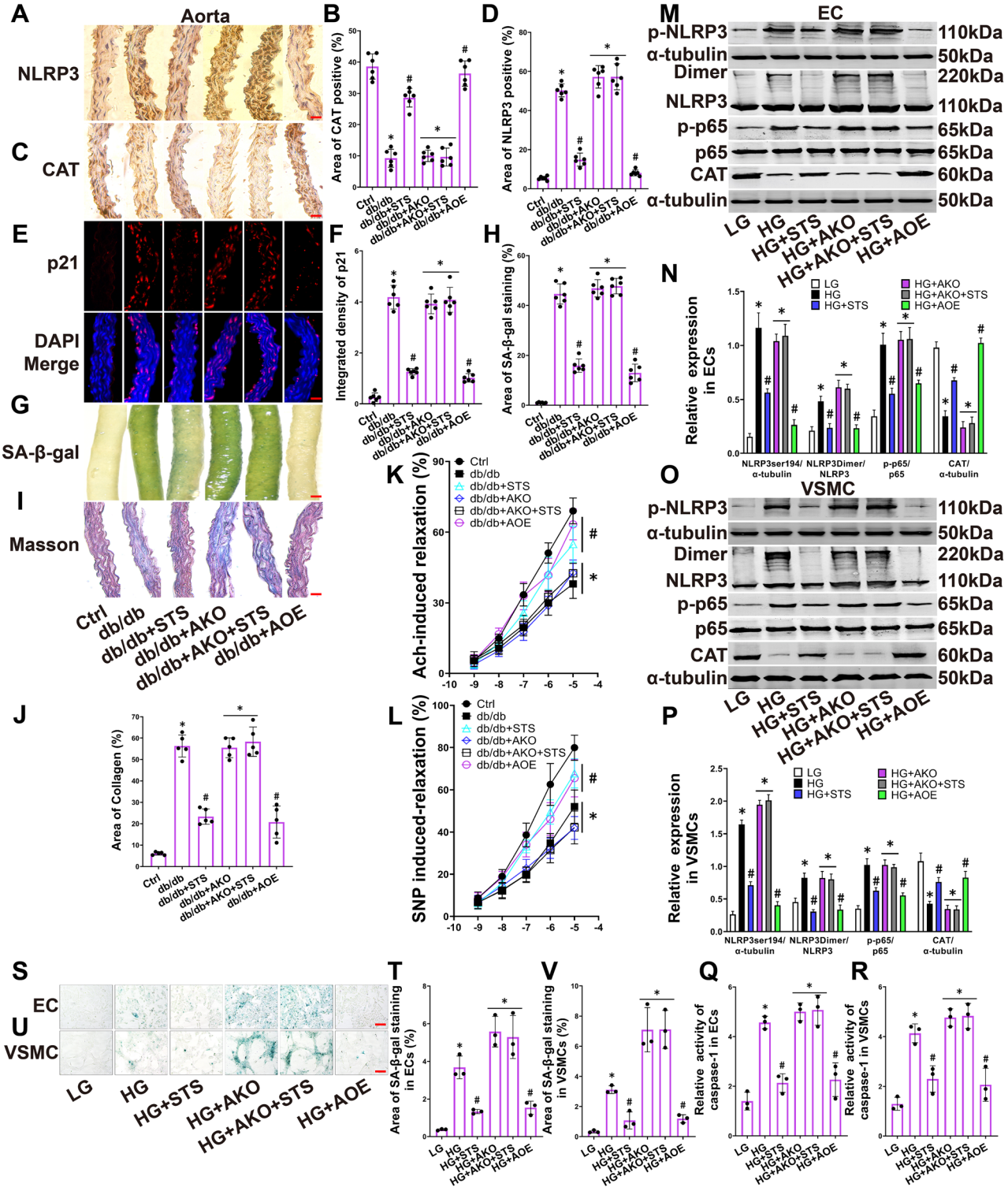

Figure 5. STS suppresses the activation of NLRP3 inflammasome and vascular senescence by activating A20 under diabetic condition. (**A**,**B**) and (**C**,**D**) Representative IHC images of NLRP3 (400×, scale bar: 20 μm) and CAT (400×, scale bar: 20 μm) and the summarized data of NLRP3 and CAT positive area percentage in aortas; (**E**,**F**) Representative immunofluorescence images of p21 (400×, scale bar: 20 μm) and the summarized data of p21 integrated density in aortas; (**G**,**H**) Representative images of SA-β-gal staining (40×, scale bar: 200 μm) and the summarized data of SA-β-gal area percentage in aortas; (**I**,**J**) Representative images of Masson staining (400×, scale bar: 20 μm) and the summarized data of collagen area percentage in aortas; (**K**,**L**) The summarized data show aortas responding to Ach and SNP; (**M**–**P**) Representative Western blot gels and summarized data show the NLRP3 phosphorylation at serine 194 site, the production of NLRP3 dimer, the phosphorylation of p65, the expression of CAT in ECs and VSMCs; (**Q**,**R**) The summarized data show the active caspase-1 in ECs and VSMCs; (**S**–**V**) Representative images of SA-β-gal staining (400×, scale bar: 20 μm) and summarized data of SA-β-gal positive area percentage in ECs and VSMCs. $^{*}P<0.05$ vs. Control (Ctrl); $^{\#}P<0.05$ vs. db/db or HG treated group (n = 6 in mice, n = 3 in cells).

was found to alleviate senescence in nucleus pulposus cells under inflammatory conditions[63]. However, the effect of A20 on senescence in ECs and VSMCs has not been established yet. Our results demonstrated that supplementing complement A20 levels reversed high glucose-induced vascular senescence, while STS limited the phosphorylation and dimerization of NLRP3 and reduced the senescence in both ECs and VSMCs through restoring A20 level. Our conclusion demonstrates the pharmacological effect of STS on vascular senescence, and our study has elucidated the mechanism of A20 protection that is connected to this effect.

Studies may suggest a possible negative correlation between the level of NLRP3 inflammasome assembly component proteins and the expression of CAT[64,65]. Our results confirmed the relationship and found that HG induced the expression of NLRP3 while inhibiting the level of CAT, and the restoration of CAT expression was observed upon knocking out NLRP3. STS possesses the pharmacological properties that exhibit anti-inflammation and anti-oxidative stress effects[59]. Additionally, early studies have implied that tanshinone IIA protected the level of CAT in nerve cells[66,67]. Despite being used as a cardiovascular medicine in clinical practice for several decades, the protective effects of STS on CAT in ECs and VSMCs under diabetic conditions remain unknown. Our results suggested that STS maintained the level of CAT and lessened the accumulation of hydrogen peroxide in ECs and VSMCs, the mechanism was related to the inhibition of NLRP3 inflammasome activation. STS may disrupt the ROS-NLRP3 inflammasome-CAT-ROS cycle by inhibiting the activation of NLRP3 inflammasome. Our conclusion provides innovative and integrative evidence for the anti-inflammatory and anti-oxidative mechanism of STS, as well as supporting its potential clinical use in the treatment of vascular disease associated with diabetes.

Notably, although STS has been reported to have vasodilatory protective effects[68,69], it has not been explored whether this protective effect is related to its alleviation of endothelial and smooth muscle cell senescence. Our results provide a preliminary description in this regard. We found that STS protects arterial vasodilation when alleviating diabetes-induced endothelial and smooth muscle cell senescence. This may indicate that diabetes-induced vascular senescence is one of the causes of impaired vascular wall relaxation capacity, and it may also suggest that the loss of vascular wall relaxation function is a marker of vascular senescence. Although we used vasodilation as one of the indirect indicators of vascular senescence in the current study, the relationship between the loss of vasodilation function and vascular senescence requires further exploration. Our results suggest that the protective effect of STS on vasodilation in diabetic animals is related to the inhibition of NLRP3 inflammasome-mediated CAT loss and the suppression of oxidative stress levels, thereby counteracting high glucose-induced endothelial and smooth muscle cell senescence.

Conclusion

Our study demonstrated that HG triggers the assembly and activation of the NLRP3 inflammasome. This process is accompanied by the phosphorylation of NLRP3 at the serine 194 site and the production of the NLRP3 dimer. HG also accelerates the senescence of ECs and VSMCs by stimulating NLRP3-dependent CAT downregulation and the accumulation of hydrogen peroxide. STS alleviates vascular oxidative stress and senescence by protecting A20 levels to inhibit the NFκB-NLRP3 pathway under diabetic conditions.

Our conclusion reveals a novel mechanism for accelerated senescence in diabetes. It also uncovers the pharmacological effect of STS in alleviating vascular senescence. This provides new basic research evidence for the potential clinical use of STS in the treatment of vascular diseases associated with diabetes.

Data availability

The datasets used and analyzed in the current study are available from the corresponding author based on reasonable request.

Received: 26 February 2024; Accepted: 22 July 2024
Published online: 26 July 2024

References

1. Burton, D. G. A. & Faragher, R. G. A. Obesity and type-2 diabetes as inducers of premature cellular senescence and ageing. *Biogerontology* **19**, 447–459. https://doi.org/10.1007/s10522-018-9763-7 (2018).
2. Chen, Y., Zhao, X. & Wu, H. Arterial stiffness: A focus on vascular calcification and its link to bone mineralization. *Arterioscler. Thromb. Vasc. Biol.* **40**, 1078–1093. https://doi.org/10.1161/atvbaha.120.313131 (2020).
3. Xu, F. *et al.* Melatonin alleviates vascular calcification and ageing through exosomal miR-204/miR-211 cluster in a paracrine manner. *J. Pineal Res.* **68**, e12631. https://doi.org/10.1111/jpi.12631 (2020).
4. Wan, Y., Liu, Z., Wu, A. & Khan, A. H. Hyperglycemia promotes endothelial cell senescence through AQR/PLAU signaling axis. *Int. J. Mol. Sci.* **23**, 2879. https://doi.org/10.3390/ijms23052879 (2022).
5. Martelli, A. & Piragine, E. The H(2)S-donor erucin exhibits protective effects against vascular inflammation in human endothelial and smooth muscle cells. *Antioxidants* **10**, 961. https://doi.org/10.3390/antiox10060961 (2021).
6. Zhang, S., An, Q., Wang, T., Gao, S. & Zhou, G. Autophagy- and MMP-2/9-mediated reduction and redistribution of ZO-1 contribute to hyperglycemia-increased blood-brain barrier permeability during early reperfusion in stroke. *Neuroscience* **377**, 126–137. https://doi.org/10.1016/j.neuroscience.2018.02.035 (2018).
7. Khemais-Benkhiat, S. *et al.* Angiotensin II-induced redox-sensitive SGLT1 and 2 expression promotes high glucose-induced endothelial cell senescence. *J. Cell. Mol. Med.* **24**, 2109–2122. https://doi.org/10.1111/jcmm.14233 (2020).
8. Zhou, D. M. *et al.* Metformin inhibits high glucose-induced smooth muscle cell proliferation and migration. *Aging* **12**, 5352–5361. https://doi.org/10.18632/aging.102955 (2020).
9. Zhong, J. Y. *et al.* LncRNA-ES3 inhibition by Bhlhe40 is involved in high glucose-induced calcification/senescence of vascular smooth muscle cells. *Ann. N. York Acad. Sci.* **1474**, 61–72. https://doi.org/10.1111/nyas.14381 (2020).
10. Li, Y. *et al.* Inhibition of vascular smooth muscle cells premature senescence with rutin attenuates and stabilizes diabetic atherosclerosis. *J. Nutr. Biochem.* **51**, 91–98. https://doi.org/10.1016/j.jnutbio.2017.09.012 (2018).

11. Yuan, T. *et al.* New insights into oxidative stress and inflammation during diabetes mellitus-accelerated atherosclerosis. *Redox Biol.* **20**, 247–260. https://doi.org/10.1016/j.redox.2018.09.025 (2019).
12. Chen, T. C. *et al.* The antagonism of 6-shogaol in high-glucose-activated NLRP3 inflammasome and consequent calcification of human artery smooth muscle cells. *Cell Biosci.* **10**, 5. https://doi.org/10.1186/s13578-019-0372-1 (2020).
13. Nyandwi, J. B. *et al.* Rosmarinic acid inhibits oxLDL-induced inflammasome activation under high-glucose conditions through downregulating the p38-FOXO1-TXNIP pathway. *Biochem. Pharmacol.* **182**, 114246. https://doi.org/10.1016/j.bcp.2020.114246 (2020).
14. Nunes, P. R., Mattioli, S. V. & Sandrim, V. C. NLRP3 activation and its relationship to endothelial dysfunction and oxidative stress: Implications for preeclampsia and pharmacological interventions. *Cells* https://doi.org/10.3390/cells10112828 (2021).
15. Kelley, N., Jeltema, D., Duan, Y. & He, Y. The NLRP3 inflammasome: An overview of mechanisms of activation and regulation. *Int. J. Mol. Sci.* https://doi.org/10.3390/ijms20133328 (2019).
16. Bai, B. *et al.* NLRP3 inflammasome in endothelial dysfunction. *Cell Death Dis.* **11**, 776. https://doi.org/10.1038/s41419-020-02985-x (2020).
17. Herrmann, J. *et al.* Stressor-induced "inflammaging" of vascular smooth muscle cells via Nlrp3-mediated pro-inflammatory auto-loop. *Front. Cardiovasc. Med.* **8**, 752305. https://doi.org/10.3389/fcvm.2021.752305 (2021).
18. Yang, H., Luo, Y. Y., Zhang, L. T., He, K. R. & Lin, X. J. Extracellular histones induce inflammation and senescence of vascular smooth muscle cells by activating the AMPK/FOXO4 signaling pathway. *Inflam. Res.* **71**, 1055–1066. https://doi.org/10.1007/s00011-022-01618-7 (2022).
19. Li, X. *et al.* Sodium tanshinone IIA silate exerts microcirculation protective effects against spinal cord injury in vitro and in vivo. *Oxid. Med. Cell. Longev.* **2020**, 3949575. https://doi.org/10.1155/2020/3949575 (2020).
20. Sun, C. *et al.* Purple sweet potato color attenuated NLRP3 inflammasome by inducing autophagy to delay endothelial senescence. *J. Cell. Physiol.* **234**, 5926–5939. https://doi.org/10.1002/jcp.28003 (2019).
21. Tai, G. J. *et al.* NLRP3 inflammasome links vascular senescence to diabetic vascular lesions. *Pharmacol. Res.* **178**, 106143. https://doi.org/10.1016/j.phrs.2022.106143 (2022).
22. Zhou, Z. Y., Zhao, W. R., Zhang, J., Chen, X. L. & Tang, J. Y. Sodium tanshinone IIA sulfonate: A review of pharmacological activity and pharmacokinetics. *Biomed. Pharmacother.* **118**, 109362. https://doi.org/10.1016/j.biopha.2019.109362 (2019).
23. Bi, Z., Wang, Y. & Zhang, W. A comprehensive review of tanshinone IIA and its derivatives in fibrosis treatment. *Biomed. Pharmacother.* **137**, 111404. https://doi.org/10.1016/j.biopha.2021.111404 (2021).
24. Zhu, J. *et al.* Tanshinone IIA Sodium sulfonate regulates antioxidant system, inflammation, and endothelial dysfunction in atherosclerosis by downregulation of CLIC1. *Eur. J. Pharmacol.* **815**, 427–436. https://doi.org/10.1016/j.ejphar.2017.09.047 (2017).
25. Zhou, Z. Y. *et al.* Sodium tanshinone IIA sulfonate promotes endothelial integrity via regulating VE-cadherin dynamics and RhoA/ROCK-mediated cellular contractility and prevents atorvastatin-induced intracerebral hemorrhage in zebrafish. *Toxicol. Appl. Pharmacol.* **350**, 32–42. https://doi.org/10.1016/j.taap.2018.04.037 (2018).
26. Xiao, X., Xu, M. & Fang, Y. Tanshinone IIA attenuates hydrogen peroxide-induced senescence of human umbilical vein endothelial cells through activating SIRT1/eNOS pathway. *Chin. J. Cell. Mol. Immunol.* **35**, 806–811 (2019).
27. Jia, S. *et al.* Tanshinone IIA attenuates high glucose induced human VSMC proliferation and migration through miR-21-5p-mediated tropomyosin 1 downregulation. *Arch. Biochem. Biophys.* **677**, 108154. https://doi.org/10.1016/j.abb.2019.108154 (2019).
28. Qin, Y. *et al.* Tanshinone IIA inhibits VSMC inflammation and proliferation in vivo and in vitro by downregulating miR-712-5p expression. *Eur. J. Pharmacol.* **880**, 173140. https://doi.org/10.1016/j.ejphar.2020.173140 (2020).
29. Wei, W., Li, X. X. & Xu, M. Inhibition of vascular neointima hyperplasia by FGF21 associated with FGFR1/Syk/NLRP3 inflammasome pathway in diabetic mice. *Atherosclerosis* **289**, 132–142. https://doi.org/10.1016/j.atherosclerosis.2019.08.017 (2019).
30. Zhang, H. *et al.* Cathelicidin hCAP18/LL-37 promotes cell proliferation and suppresses antitumor activity of 1,25(OH)(2)D(3) in hepatocellular carcinoma. *Cell Death Discov.* **8**, 27. https://doi.org/10.1038/s41420-022-00816-w (2022).
31. Shen, X. *et al.* CircRILPL1 promotes muscle proliferation and differentiation via binding miR-145 to activate IGF1R/PI3K/AKT pathway. *Cell Death Dis.* **12**, 142. https://doi.org/10.1038/s41419-021-03419-y (2021).
32. Tan, X. *et al.* Tanshinone IIA protects against cardiac hypertrophy via inhibiting calcineurin/NFATc3 pathway. *Int. J. Biol. Sci.* **7**, 383–389. https://doi.org/10.7150/ijbs.7.383 (2011).
33. Maione, F. *et al.* Down regulation of pro-inflammatory pathways by tanshinone IIA and cryptotanshinone in a non-genetic mouse model of Alzheimer's disease. *Pharmacol. Res.* **129**, 482–490. https://doi.org/10.1016/j.phrs.2017.11.018 (2018).
34. Gao, Q. *et al.* Effects of the NF-κB signaling pathway inhibitor BAY11–7082 in the replication of ASFV. *Viruses* https://doi.org/10.3390/v14020297 (2022).
35. Luo, X., Wang, R., Lv, C. & Chen, G. Detection of selenocysteine with a ratiometric near-infrared fluorescent probe in cells and in mice thyroid diseases model. *Anal. Chem.* **92**, 1589–1597. https://doi.org/10.1021/acs.analchem.9b04860 (2020).
36. Ma, W. *et al.* Ultra-efficient antibacterial system based on photodynamic therapy and CO gas therapy for synergistic antibacterial and ablation biofilms. *ACS Appl. Mater. Interfaces* **12**, 22479–22491. https://doi.org/10.1021/acsami.0c01967 (2020).
37. Xu, M. *et al.* TRPV1 and TRPA1 in lung inflammation and airway hyperresponsiveness induced by fine particulate matter (PM(2.5)). *Oxid. Med. Cell. Longev.* **2019**, 7450151. https://doi.org/10.1155/2019/7450151 (2019).
38. Hu, R. *et al.* Salidroside ameliorates endothelial inflammation and oxidative stress by regulating the AMPK/NF-κB/NLRP3 signaling pathway in AGEs-induced HUVECs. *Eur. J. Pharmacol.* **867**, 172797. https://doi.org/10.1016/j.ejphar.2019.172797 (2020).
39. Martens, A. & van Loo, G. A20 at the Crossroads of Cell Death, Inflammation, and Autoimmunity. *Cold Spring Harbor Perspect. Biol.* **12**, a036418. https://doi.org/10.1101/cshperspect.a036418 (2020).
40. Feng, J. *et al.* The protective effect of tanshinone IIa on endothelial cells: A generalist among clinical therapeutics. *Expert Rev. Clin. Pharmacol.* **14**, 239–248. https://doi.org/10.1080/17512433.2021.1878877 (2021).
41. Liu, S. Y. *et al.* Role of vascular peroxidase 1 in senescence of endothelial cells in diabetes rats. *Int. J. Cardiol.* **197**, 182–191. https://doi.org/10.1016/j.ijcard.2015.06.098 (2015).
42. Zhu, S. L. *et al.* Capsaicin ameliorates intermittent high glucose-mediated endothelial senescence via the TRPV1/SIRT1 pathway. *Phytomedicine* **100**, 154081. https://doi.org/10.1016/j.phymed.2022.154081 (2022).
43. Zhang, M. *et al.* Both high glucose and phosphate overload promote senescence-associated calcification of vascular muscle cells. *Int. Urol. Nephrol.* **54**, 2719–2731. https://doi.org/10.1007/s11255-022-03195-4 (2022).
44. Zhang, J. *et al.* Stachydrine ameliorates carbon tetrachloride-induced hepatic fibrosis by inhibiting inflammation, oxidative stress and regulating MMPs/TIMPs system in rats. *Biomed. Pharmacother.* **97**, 1586–1594. https://doi.org/10.1016/j.biopha.2017.11.117 (2018).
45. Zhang, B. *et al.* SIRT3 overexpression antagonizes high glucose accelerated cellular senescence in human diploid fibroblasts via the SIRT3-FOXO1 signaling pathway. *Age (Dordrecht, Netherlands)* **35**, 2237–2253. https://doi.org/10.1007/s11357-013-9520-4 (2013).
46. Lin, Q. *et al.* PINK1-parkin pathway of mitophagy protects against contrast-induced acute kidney injury via decreasing mitochondrial ROS and NLRP3 inflammasome activation. *Redox Biol.* **26**, 101254. https://doi.org/10.1016/j.redox.2019.101254 (2019).
47. Han, X. *et al.* Quercetin hinders microglial activation to alleviate neurotoxicity via the interplay between NLRP3 inflammasome and mitophagy. *Redox Biol.* **44**, 102010. https://doi.org/10.1016/j.redox.2021.102010 (2021).

48. Pang, Q. & Wang, P. Irisin protects against vascular calcification by activating autophagy and inhibiting NLRP3-mediated vascular smooth muscle cell pyroptosis in chronic kidney disease. *Cell Death Dis.* **13**, 283. https://doi.org/10.1038/s41419-022-04735-7 (2022).
49. Naeem, A. G., El-Naga, R. N. & Michel, H. E. Nebivolol elicits a neuroprotective effect in the cuprizone model of multiple sclerosis in mice: Emphasis on M1/M2 polarization and inhibition of NLRP3 inflammasome activation. *Inflammopharmacology* **30**, 2197–2209. https://doi.org/10.1007/s10787-022-01045-4 (2022).
50. Wang, M. *et al.* Roles of TRPA1 and TRPV1 in cigarette smoke -induced airway epithelial cell injury model. *Free Radical Biol. Med.* **134**, 229–238. https://doi.org/10.1016/j.freeradbiomed.2019.01.004 (2019).
51. Huang, D., Gao, W., Zhong, X. & Ge, J. NLRP3 activation in endothelia promotes development of diabetes-associated atherosclerosis. *Aging* **12**, 18181–18191. https://doi.org/10.18632/aging.103666 (2020).
52. Swanson, K. V. & Deng, M. The NLRP3 inflammasome: Molecular activation and regulation to therapeutics. *Nat. Rev. Immunol.* **19**, 477–489. https://doi.org/10.1038/s41577-019-0165-0 (2019).
53. Huang, Y. *et al.* Tranilast directly targets NLRP3 to treat inflammasome-driven diseases. *EMBO Mol. Med.* https://doi.org/10.15252/emmm.201708689 (2018).
54. Hou, F. *et al.* MAVS forms functional prion-like aggregates to activate and propagate antiviral innate immune response. *Cell* **146**, 448–461. https://doi.org/10.1016/j.cell.2011.06.041 (2011).
55. Li, T. *et al.* Overproduction of gastrointestinal 5-HT promotes colitis-associated colorectal cancer progression via enhancing NLRP3 inflammasome activation. *Cancer Immunol. Res.* **9**, 1008–1023. https://doi.org/10.1158/2326-6066.cir-20-1043 (2021).
56. Li, Y. *et al.* Tanshinone IIA alleviates NLRP3 inflammasome-mediated pyroptosis in Mycobacterium tuberculosis-(H37Ra-) infected macrophages by inhibiting endoplasmic reticulum stress. *J. Ethnopharmacol.* **282**, 114595. https://doi.org/10.1016/j.jep.2021.114595 (2022).
57. Wen, J. *et al.* Tanshinone IIA attenuates atherosclerosis via inhibiting NLRP3 inflammasome activation. *Aging* **13**, 910–932. https://doi.org/10.18632/aging.202202 (2020).
58. Chen, P., An, Q., Huang, Y., Zhang, M. & Mao, S. Prevention of endotoxin-induced cardiomyopathy using sodium tanshinone IIA sulfonate: Involvement of augmented autophagy and NLRP3 inflammasome suppression. *Eur. J. Pharmacol.* **909**, 174438. https://doi.org/10.1016/j.ejphar.2021.174438 (2021).
59. Zhu, J., Chen, H., Guo, J., Zha, C. & Lu, D. Sodium tanshinone IIA sulfonate inhibits vascular endothelial cell pyroptosis via the AMPK signaling pathway in atherosclerosis. *J. Inflamm. Res.* **15**, 6293–6306. https://doi.org/10.2147/jir.s386470 (2022).
60. Xue, Z. *et al.* miR-21 promotes NLRP3 inflammasome activation to mediate pyroptosis and endotoxic shock. *Cell Death Dis.* **10**, 461. https://doi.org/10.1038/s41419-019-1713-z (2019).
61. Mouton-Liger, F. *et al.* Parkin deficiency modulates NLRP3 inflammasome activation by attenuating an A20-dependent negative feedback loop. *Glia* **66**, 1736–1751. https://doi.org/10.1002/glia.23337 (2018).
62. Cheng, L. *et al.* Decreased A20 mRNA and protein expression in peripheral blood mononuclear cells in patients with type 2 diabetes and latent autoimmune diabetes in adults. *Diabetes Res. Clin. Pract.* **106**, 611–616. https://doi.org/10.1016/j.diabres.2014.09.014 (2014).
63. Peng, X. *et al.* A20 of nucleus pulposus cells plays a self-protection role via the nuclear factor-kappa B pathway in the inflammatory microenvironment. *Bone Jt. Res.* **9**, 225–235. https://doi.org/10.1302/2046-3758.95.bjr-2019-0230.r1 (2020).
64. Yang, C., Xia, W., Liu, X., Lin, J. & Wu, A. Role of TXNIP/NLRP3 in sepsis-induced myocardial dysfunction. *Int. J. Mol. Med.* **44**, 417–426. https://doi.org/10.3892/ijmm.2019.4232 (2019).
65. Ding, T. *et al.* Vitexin exerts protective effects against calcium oxalate crystal-induced kidney pyroptosis in vivo and in vitro. *Phytomedicine* **86**, 153562. https://doi.org/10.1016/j.phymed.2021.153562 (2021).
66. Liu, Y. *et al.* Tanshinone IIA improves impaired nerve functions in experimental diabetic rats. *Biochem. Biophys. Res. Commun.* **399**, 49–54. https://doi.org/10.1016/j.bbrc.2010.07.037 (2010).
67. Li, H. *et al.* Tanshinone IIA inhibits glutamate-induced oxidative toxicity through prevention of mitochondrial dysfunction and suppression of MAPK activation in SH-SY5Y human neuroblastoma cells. *Oxid. Med. Cell. Longev.* **2017**, 4517486. https://doi.org/10.1155/2017/4517486 (2017).
68. Zhou, Y. *et al.* Decreased vasodilatory effect of Tanshinone IIA Sodium Sulfonate on mesenteric artery in hypertension. *Eur. J. Pharmacol.* **854**, 365–371. https://doi.org/10.1016/j.ejphar.2019.04.049 (2019).
69. Tan, X. Q. *et al.* Tanshinone II-A sodium sulfonate (DS-201) enhances human BKCa channel activity by selectively targeting the pore-forming α subunit. *Acta Pharmacologica Sinica* **35**, 1351–1363. https://doi.org/10.1038/aps.2014.85 (2014).

Author contributions

WW and HYY: equally, laboratory work, data analysis and interpretation, manuscript writing, and financial support; WFF: laboratory work and financial support; LJX, LCY, YBJ, LXY, FJN, ZPF, DHY: laboratory work and administrative support; WW: conception and study design and final approval of the manuscript. All authors have read and approved the manuscript.

Funding

This work was supported by Youth Project of Heping Hospital Affiliated to Changzhi Medical College (HPYJ201921, HPYJ202218); Scientific and Technological Innovation Programs (STIP) of Higher Education Institutions in Shanxi (2021L351); the research fund of Changzhi Medical College (BS202115) and the grants from Department of Science and Technology of Shanxi (202203021211107), the grants from Health Commission of Shanxi Province (2022021); funding from Professor Qifu Li'sworkstation in Shanxi Province.

Competing interests

The authors declare no competing interests.

Additional information

Supplementary Information The online version contains supplementary material available at https://doi.org/10.1038/s41598-024-68169-1.

Correspondence and requests for materials should be addressed to W.W.